

Simultaneously tunable luminescence and magnetic properties in bifunctional $\text{NaYF}_4: \text{Yb}^{3+}/\text{Er}^{3+}$ microcrystals

Zhijun Tang^{a,*}, Quan Liu^a, Xiaofeng Wu^a, Shigang Hu^a, Zaifang Xi^a, Shiping Zhan^b, Yunxin Liu^{b,*}

^a School of Information and Electrical Engineering, Hunan University of Science and Technology, Xiangtan 411201 China

^b School of Physics and Electronic Science, Hunan University of Science and Technology, Xiangtan 411201 China

*Corresponding authors, e-mail: zjtang@hnust.edu.cn, lyunxin@163.com

Received 15 Aug 2019

Accepted 23 Apr 2020

ABSTRACT: A series of bifunctional NaYF_4 microcrystals doped with $\text{Yb}^{3+}/\text{Er}^{3+}$ have been successfully synthesized through a facile hydrothermal method. They have been characterized by XRD, SEM, photoluminescence spectra and the magnetization. These microcrystals can emit ~ 540 nm green light from Er^{3+} - $4f^n$ electronic transition $^4S_{3/2}$ - $^4I_{15/2}$, ~ 657 nm red light from Er^{3+} - $4f^n$ electronic transition $^4F_{9/2}$ - $^4I_{15/2}$, and ~ 407 nm violet light from Er^{3+} - $4f^n$ electronic transition $^2H_{9/2}$ - $^4I_{15/2}$, under the excitation of 980 nm infrared light. It is found that the red emission is more sensitive to the doping of Yb^{3+} ion than the green one, leading to the significant increase in the ratio of red emission to green emission with increasing concentration of Yb^{3+} ion. In addition, the paramagnetic property was remarkably enhanced with increasing concentration of Yb^{3+} ion which is ascribed to the substitution of nonmagnetic ion Y^{3+} by the magnetic ion Yb^{3+} with large magnetic moment.

KEYWORDS: up-conversion luminescence, bifunctional microcrystals, magnetic property, heavy doping

INTRODUCTION

Up-conversion (UC) materials are those materials that can convert near-infrared emission into visible or ultra-violet emission. They have wide spread applications in various fields such as bio-sensors, bio-imaging, environment monitoring [1, 2], information storage [3, 4], anti-counterfeiting [5–7] and solar cells [8, 9], and thus attracted a tremendous amount of attention for the past decade [10–12]. These trivalent lanthanide-doped ions have unique spectral and magnetic properties and a broad application prospects in many areas [13, 14].

As well known, the light-emitting properties of rare earth and host materials are associated with the doping concentration of rare earth ions and other factors. Among all up-conversion materials [15, 16], $\text{NaYF}_4: \text{Yb}^{3+}/\text{Er}^{3+}$ has been deemed to be the most efficient infrared-to-visible up-conversion phosphors. In the recent years, the control synthesis of morphology, crystal phase, particle size, and core/shell structure has been developed for NaYF_4 up-conversion micro-crystals and nanoparticles, while their up-conversion

luminescent characteristics are well investigated accompanied with the detailed demonstration of energy transfer mechanisms [17, 18]. Recently, optical-magnetic bifunctional materials constructed by combining up-conversion luminescent materials with magnetic ones have attracted increasing attentions. Examples are: core-shell $\text{NaYF}_4: \text{Yb}^{3+}/\text{Tm}^{3+}@\text{Fe}_3\text{O}_4$ nanocrystals for dual-modality T_2 -enhanced magnetic resonance and NIR-to-NIR up-conversion luminescent imaging of small-animal lymphatic node [19], super-paramagnetic and up-conversion emitting of $\text{Fe}_3\text{O}_4/\text{NaYF}_4: \text{Yb}^{3+}/\text{Er}^{3+}$ hetero-nanoparticles via a crosslinker anchoring strategy [20], core-shell $\text{Fe}_3\text{O}_4@\text{NaLuF}_4: \text{Yb}^{3+}/\text{Er}^{3+}/\text{Tm}^{3+}$ nanostructure with multifunctional properties synthesized by a step-wise synthetic method [21], and MWCNTs/ $\text{NaGdF}_4: \text{Yb}^{3+}/\text{Er}^{3+}$ nanocomposites synthesized by a simple liquid method with good paramagnetic, up-conversion luminescence, photothermal properties and biocompatibility [22]. However, these bifunctional materials are actually the mixture of optical materials and magnetic ones which have some intrinsic problems, such as optical

and magnetic phase-separation and non-uniform optical and magnetic properties.

More recently, $\text{Er}^{3+}/\text{Yb}^{3+}$ doped NaGdF_4 bifunctional nanocrystals with optimizing fluorescent and paramagnetic properties were successfully grown in our laboratory [23]. Furthermore, $\text{Er}^{3+}/\text{Yb}^{3+}$ doped NaLuF_4 bifunctional microcrystals co-doped with Gd^{3+} or Dy^{3+} were also successfully synthesized and enhanced up-conversion luminescence and ferromagnetic-paramagnetic transition [24].

In this work, the $\text{NaYF}_4:\text{Yb}^{3+}/\text{Er}^{3+}$ bifunctional microcrystals were successfully synthesized by a facile hydrothermal method, and their optical and magnetic properties could be simultaneously tuned by changing the doping level of $\text{Yb}^{3+}/\text{Er}^{3+}$. Furthermore, the co-doping of magnetic ion $\text{Yb}^{3+}/\text{Er}^{3+}$ affects the magnetic property of NaYF_4 through heavy doping. Meanwhile, the heavy doping of Yb^{3+} ion would change the crystal field environment of emitter Er^{3+} so that the up-conversion emission of $\text{NaYF}_4:\text{Yb}^{3+}/\text{Er}^{3+}$ changes correspondingly. By analyzing the crystal structure, the fluorescence properties, and the dependence of magnetization on the applied magnetic field, simultaneous tuning of up-conversion luminescence and magnetic property in NaYF_4 crystal was investigated.

MATERIALS AND METHODS

Materials

Rare-earth (RE) oxides including YO_2 (99.9%), YbO_2 (99.9%) and ErO_2 (99%); trisodium citrate (99%), sodium fluoride (NaF), and nitric acid (HNO_3), were all purchased from Sinopharm Chemical Reagent Company of China. Deionized water was used throughout. Unless otherwise noted, all chemicals were used directly without further purification.

Synthesis

Here, $\text{NaYF}_4:18\%\text{Yb}^{3+}/x\%\text{Er}^{3+}$ ($x = 2, 12, 22$ and 32 mol%), and $\text{NaYF}_4:x\%\text{Yb}^{3+}/2\%\text{Er}^{3+}$ ($x = 18, 38, 58$ and 78 mol%) microcrystals were synthesized by the hydrothermal method using trisodium citrate as stabilizing surfactant. Firstly, 0.35 g of trisodium citrate and 10 ml of distilled water were firstly mixed together under agitation to form a homogeneous solution. Then, in a mixing state, added 1.2 ml (0.5 mmol/ml) of $\text{Y}(\text{NO}_3)_3$ solution to each drop, and continue stirring for 10 minutes. Then, in a mixing state, 20 ml (0.35 mmol/ml) of NaF aqueous solution were added dropwise. The solution was transferred to a 50 ml stainless steel autoclave and

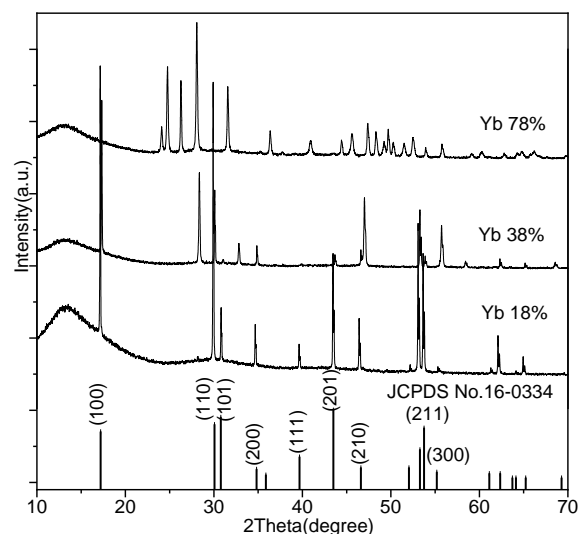


Fig. 1 XRD patterns of the $\text{NaYF}_4:x\%\text{Yb}^{3+}, 2\%\text{Er}^{3+}$ ($x = 18\%, 38\%, 78\%$).

heated at 180°C for 10 h, then the autoclave was cooled down to room temperature naturally. The samples were washed three times by the mixture of ethanol and distilled water, accompanied with centrifugal separation in order to remove other residual solvents. Finally, these samples were dried at 60°C for 24 h in a loft drier.

Characterization

X-ray power diffraction (XRD) patterns were performed using a Bruker/AXS D8-ADVANCE X-ray diffractometer equipped with a copper target ($\lambda = 1.541$ nm) for 2θ range from 10° to 70° by a step of 0.02° . Scanning electron microscope (SEM) images were recorded on a ZEISS EVO18 scanning electron microscope. Up-conversion emission spectra of these samples were recorded with a Hitachi F-2700 fluorescence spectrophotometer, while the pump excitation source for characterization was an external 980 nm semiconductor laser. The magnetization of these NaYF_4 microcrystals was recorded using a Lake-shore 7307 vibrating sample magnetometer.

RESULTS AND DISCUSSION

Crystal structure

XRD patterns of $\text{NaYF}_4:\text{Yb}^{3+}/\text{Er}^{3+}$ with different Yb^{3+} ion concentration are shown in Fig. 1. All diffraction peaks of the $\text{NaLuF}_4:18\%\text{Yb}^{3+}, 2\%\text{Er}^{3+}$ sample match very well with the standard diffraction peaks of hexagonal phase structure NaYF_4 (Joint Committee for Powder Diffraction

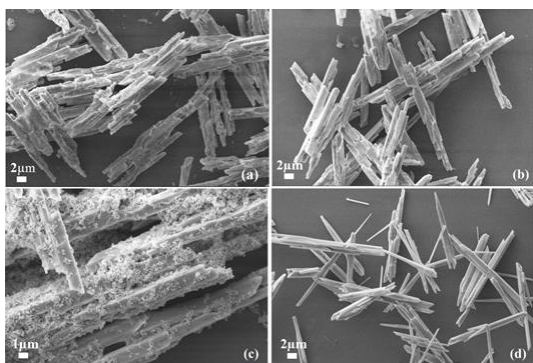


Fig. 2 SEM image of $\text{NaYF}_4: 18\% \text{Yb}^{3+}, x\% \text{Er}^{3+}$ samples: (a) $x = 2$, (b) $x = 12$, (c) $x = 22$, (d) $x = 32$.

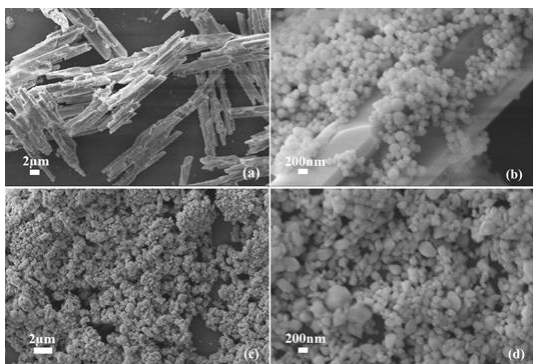


Fig. 3 SEM image of $\text{NaYF}_4: x\% \text{Yb}^{3+}, 2\% \text{Er}^{3+}$ samples: (a) $x = 18$, (b) $x = 38$, (c) $x = 58$, (d) $x = 78$.

Studies (JCPDS) card 16-0334). It can also be seen from Fig. 1 that a small quantity of diffraction peaks corresponding to cubic-phase NaYF_4 are observed when the Yb^{3+} concentration is changed from 18 mol% to 38 mol%. Furthermore, many diffraction peaks corresponding to cubic-phase NaYF_4 are observed when the Yb^{3+} ion concentration are changed from 38 mol% to 78 mol%. This means that with the increase of the Yb^{3+} ion concentration, more cubic-phase NaYF_4 crystals are mixed with the hexagonal phase NaYF_4 crystals, and this phenomenon is more obvious when the Yb^{3+} ions are doped heavily.

To further reveal the phase and size control, these prepared microcrystals were measured by a ZEISS EVO18 SEM. On the one hand, the Yb^{3+} ion concentration was held constant (18 mol%), while that of Er^{3+} ions was changed. It is observed in Fig. 2 that the NaYF_4 microcrystals with different

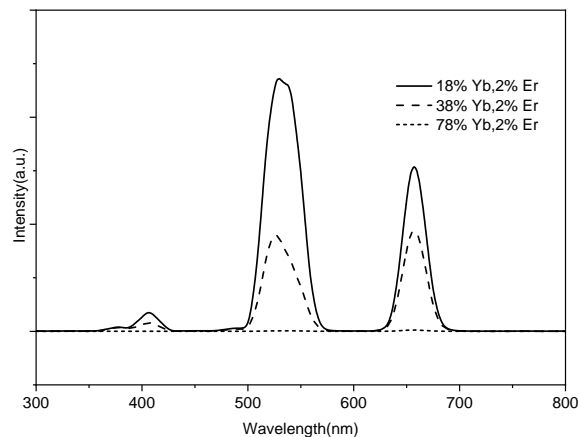


Fig. 4 Up-conversion luminescence spectra of NaYF_4 samples with different Yb^{3+} ion concentration.

Er^{3+} ion concentration have the shape of relatively regular hexagonal rods. With the increasing of Er^{3+} ion concentration from 2 mol% to 32 mol%, the diameter of these rods are gradually reduced, while the length of the rods are gradually increased. In addition, when the Er^{3+} concentration is 22 mol%, the NaYF_4 microcrystals have the shape of hexagonal rods and microplates. On the other hand, the Yb^{3+} concentration was held constant (2 mol%), while that of Yb^{3+} ions was changed. It is clear in Fig. 3 that these NaYF_4 crystals morphology change with different Yb^{3+} ion concentration. Furthermore, with the increasing of Yb^{3+} ion concentration from 18 mol% to 38 mol%, the NaYF_4 microcrystals have the shape of hexagonal rods and microplates mixing with some cubic-phase microplates. Especially, when the Yb^{3+} are doped heavily (58 mol% or 78 mol% Yb^{3+}), the size of the NaYF_4 microcrystals is reduced and the crystals have the shape of hexagonal mixed with many cubic-phase microplates. These are consistent with the results of the above-mentioned XRD diffraction analysis. Usually, the difference in morphology may lead to the differential surface properties [25, 26]. On the other hand, the up-conversion emission is highly dependent on the surface properties [27, 28]. Then, it can inferred that the up-conversion emissions of the samples doped with 18 mol% Yb^{3+} ions are different from the other two samples. This suggestion is confirmed by the following fluorescent spectra.

UC luminescence properties

The up-conversion fluorescence spectra of these samples were measured with a Hitachi F-2700 spec-

trophotometer, which are shown in Fig. 4–Fig. 6. From the up-conversion emission spectra of $\text{NaYF}_4: x\% \text{Yb}^{3+} / 2\% \text{Er}^{3+}$ ($x = 18, 38$ and 78) (Fig. 4), we can observe emission of violet, green and red at ~ 407 , ~ 540 and ~ 557 nm, respectively. When Yb^{3+} ion concentration is 18%, emission peak from high to low is green, red and violet, respectively. It can be seen that with the increase of Yb^{3+} ion concentration from 18% to 38%, the intensity of red emission increases while that of green emission decreases. The change of emission intensity can be explained by the change of distance between Er^{3+} and Yb^{3+} . With the increase of the concentration of Yb^{3+} ion in the host lattice, the average distance between Er^{3+} and Yb^{3+} decreases, and the energy transfer from Er^{3+} to Yb^{3+} will be more effective. However, the back energy transfer suppresses the excited state of energetic ions, which decreases the intensity of violet and green emission, and increases the emission intensity of red light. Furthermore, when Yb^{3+} ion concentration changes from 38% to 78%, the light intensity decreased significantly and the concentration was quenched as the distance between Yb^{3+} decreases further. In addition, the ratio of the red peak to the green wave crest is further increased due to the enhancement of the inverse energy transfer.

Fig. 5 showed the up-conversion luminescence spectra of $\text{NaYF}_4: x\% \text{Yb}^{3+} / 2\% \text{Er}^{3+}$ ($x = 18, 38$ and 78) excited with a 980 nm laser operating at four different powers. With the increase of the excited power, all emission intensity of violet, green and red are enhanced for three different $\text{Yb}^{3+} / \text{Er}^{3+}$ doping. But the changes of three kind of emission intensity are different. For emission spectra of the $\text{NaYF}_4: 18\% \text{Yb}^{3+} / 2\% \text{Er}^{3+}$ shown in Fig. 5a, the violet and green emission intensity increase almost proportionally with the power of excitation. When the excited power increases from 150 to 550 mW, red emission intensity is also enhanced almost proportionally with the power of excitation. However, when the excited power increases from 550 to 750 mW, the increase of red emission intensity is very small. For emission spectra of the $\text{NaYF}_4: 38\% \text{Yb}^{3+} / 2\% \text{Er}^{3+}$ shown in Fig. 5b, the three kinds of emission intensity increase significantly when the excited power increases from 150 to 340 mW. However, the increase of luminous intensity is not obvious when the excitation power continues to be increased. For emission spectra of the $\text{NaYF}_4: 78\% \text{Yb}^{3+} / 2\% \text{Er}^{3+}$ shown in Fig. 5c, except for the violet emission, the green and red emission intensity

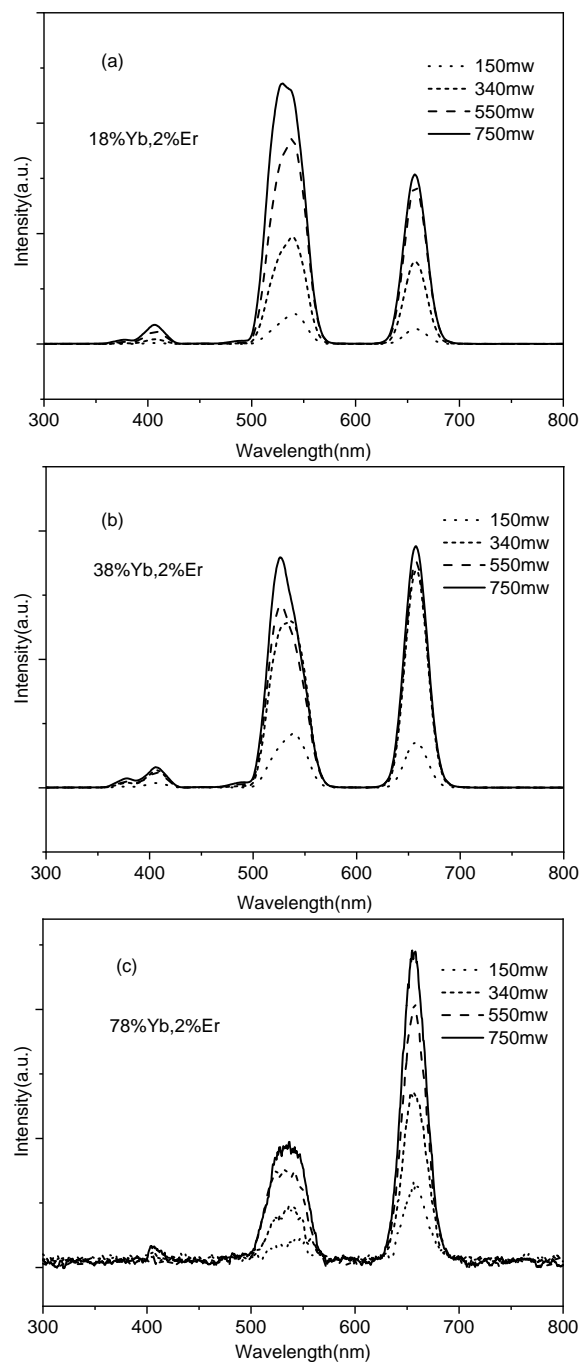


Fig. 5 Up-conversion luminescence spectra of NaYF_4 samples with different Yb^{3+} ion concentration, excited with a 980 nm laser operating at different power.

increase proportionally with the power of excitation.

In order to investigate the relationships among the three kinds of fluorescence, we assume that the green emission intensities of the three different Yb^{3+} ion doping are the same. Then the changes

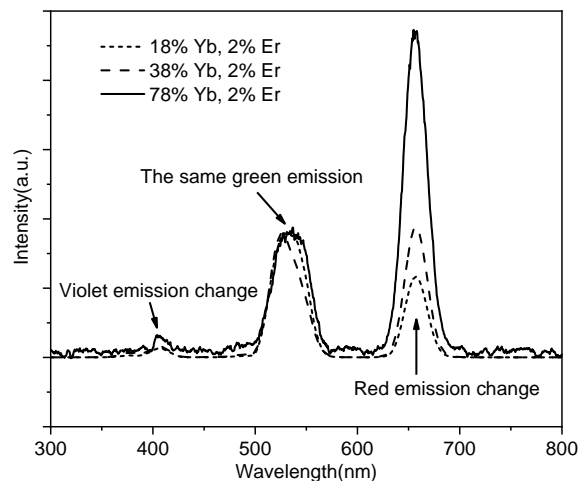


Fig. 6 Changes in the red and violet emission intensity when green emission intensity is the same.

of the violet and red emission are obtained, which are shown in Fig. 6. It is observed that the violet emission is less affected by either Yb^{3+} light doping (18%) or Yb^{3+} heavy doping (38%, 78%). However, the red emission is more affected by the Yb^{3+} ion doping concentration. With the increase of Yb^{3+} doping concentration, the ratio of red to green emission increases significantly.

To further understand the populating mechanism of the excited states following near infrared irradiation, the up-conversion luminescence intensities versus the excitation power density were performed. As we all know, for the unsaturated UC process, the number of photons needed to generate photons can be obtained by the following formula

$$I_f \propto P^n \quad (1)$$

Where I_f is the fluorescent intensity, P^n is the pump laser power, and n is the number of the laser photons required. The excitation power dependence of the green and red emission bands for NaYF_4 microcrystals was measured, and treated by Auzel's method. The green emission intensity as a function of excitation power is shown in Fig. 7a. The parameters n for the 18%, 38% and 78% Yb^{3+} doping equal to 1.36, 0.87 and 0.90, respectively. The n value of 18% Yb^{3+} doping for green emission is observed in the range of 1–2, which corresponds to the two-photon conversion process. The n value of 1.36 means that the two-photon process is involved in the generation of near infrared emission.

The n value of 38% Yb^{3+} doping is below 1, which is seemingly impossible. In fact, due to the

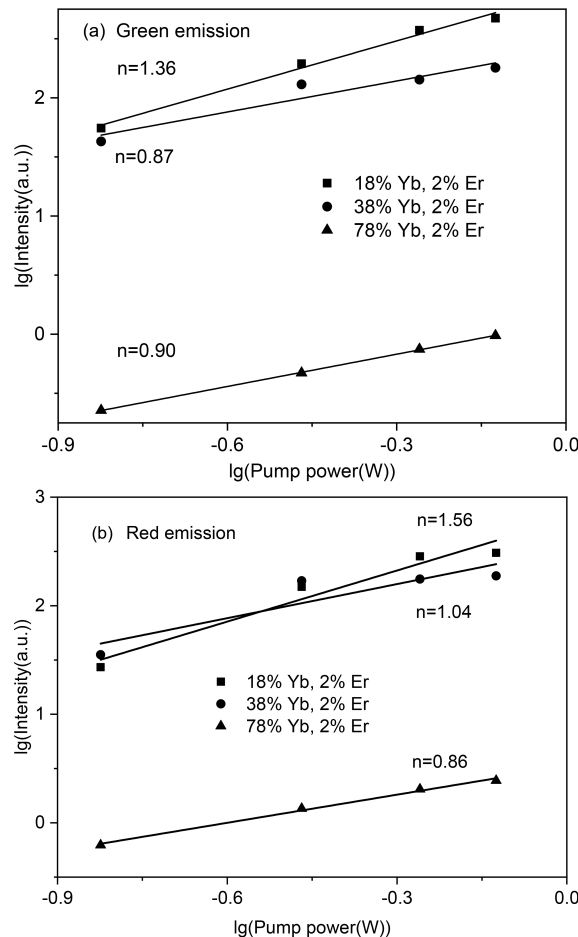


Fig. 7 The emission intensity as a function of excitation power. (a) Green emission (b) Red emission

increase of Yb^{3+} ion, the energy delivered by Yb^{3+} to Er^{3+} increases, so that the ${}^4I_{11/2}$ level is saturated with electrons. At this time, only one electron can be absorbed, and it can jump to the ${}^4I_{7/2}$ level and then releases green emission.

The n value of 78% Yb^{3+} doping is about the same as that of 38% Yb^{3+} doping, indicating that the energy levels of ${}^4I_{11/2}$ are already saturated at the 38% Yb^{3+} doping, and that the addition of more Yb^{3+} ions does not further reduce n value.

The red emission intensity as a function of excitation power is shown in Fig. 7b. The parameters n for the 18, 38% and 78% Yb^{3+} doping equal to 1.56, 1.04 and 0.86, respectively. This is similar to green emission, with increase of Yb^{3+} doping ratio, n value decreases. When the value of n is in the range of 1 to 2, the process of two-photon conversion happens. When n value is less than 1, the level of ${}^4I_{11/2}$ is already saturated. only need one

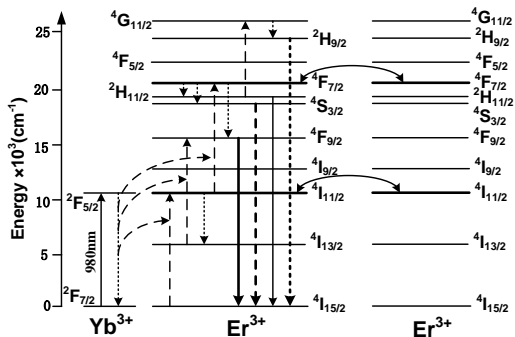


Fig. 8 Energy level diagrams and the relative transitions of Er³⁺ and Yb³⁺.

photon, one Er³⁺ transits from level ⁴I_{11/2} to level ⁴I_{7/2}, then exchanges energy with another level in ⁴I_{11/2} Er³⁺, and enters into two levels of ⁴I_{9/2}, and then emits red light.

In the Yb³⁺/Er³⁺ co-doped materials, the up-conversion luminescence involved in multi-step excited state absorption, energy transfer of excited state Er³⁺ ions, and the continuous up-conversion energy transfer between Yb³⁺ ions and Er³⁺ ions. According to the energy matching and two or three photon processes depending on the excitation power, possible mechanism for the up-conversion emission is presented based on the simplified energy level diagrams of Yb³⁺ and Er³⁺ ions in Fig. 8. The detailed transition processes are described as follow.

As shown in Fig. 4, violet, green and red emissions are observed at ~407 nm, ~540 nm (and weak green emission ~520 nm), and ~657 nm, respectively. For the energy transfer and the relative transitions of Er³⁺ and Yb³⁺, Yb³⁺ ion is first excited by a pump photon at 980 nm, the ²F_{7/2} ground state level transits to the ²F_{5/2} excited state level (²F_{7/2} → ²F_{5/2}), then Yb³⁺ ion transfers the energy to the neighboring Er³⁺ ion, so that the ⁴I_{15/2} ground state of Er³⁺ ion transits to the ⁴I_{11/2} excited state level, and at the same time Yb³⁺ ions return to the ground state (²F_{5/2}(Yb³⁺) + ⁴I_{15/2}(Er³⁺) → ²F_{7/2}(Yb³⁺) + ⁴I_{11/2}(Er³⁺)). Subsequently, Yb³⁺ ions can transfer the energy to Er³⁺ ions again through the same process, and then it is further transited from the energy ⁴I_{11/2} level to the ⁴F_{7/2} level (²F_{5/2}(Yb³⁺) + ⁴I_{11/2}(Er³⁺) → ²F_{7/2}(Yb³⁺) + ⁴I_{7/2}(Er³⁺)). The ⁴F_{7/2} level non-radiatively relaxes to the ⁴S_{3/2} low-energy excited state level, Er³⁺

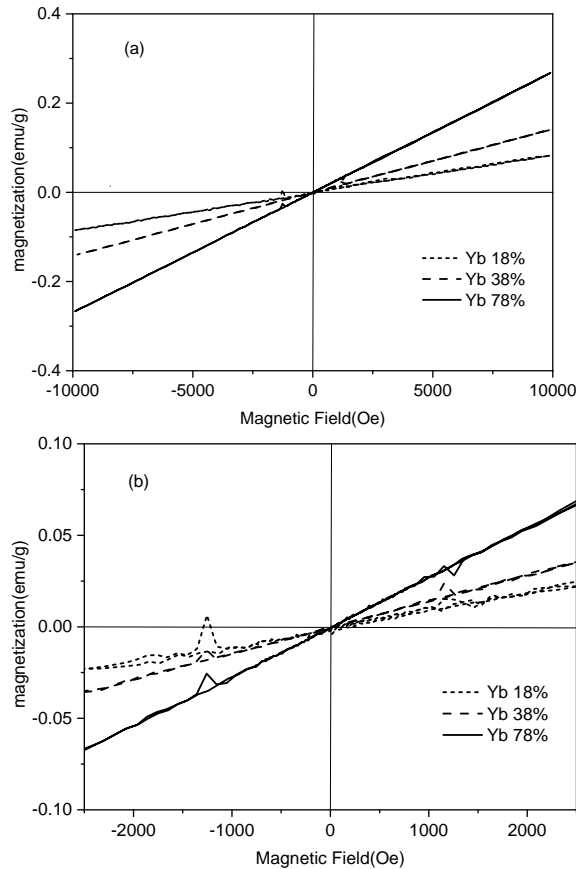


Fig. 9 Dependence of magnetization on the applied magnetic field (from -10 kOe to 10 kOe) for NaYF₄: x%Yb³⁺, 2%Er³⁺ microcrystals (x = 18, 38, 78 mol%).

followed by ⁴S_{3/2} level radiation photon returns to the ground state of ⁴I_{15/2} level, leading to stronger green light emission at the wavelength of ~540 nm. In addition, The ⁴F_{7/2} level non-radiatively relaxes to the ²H_{11/2} low-energy excited state level, leading to the weak green emission centered ~520 nm from the transition ²H_{11/2}-⁴I_{15/2}. On the other hand, the ⁴F_{7/2} level can non-radiatively relax to ⁴F_{9/2} level, and then the ⁴F_{9/2} level radiates photon and returns to the ⁴I_{15/2} ground state level, leading to red light emission at the wavelength of ~657 nm. Furthermore, the ²H_{11/2} level can be excited to the higher ⁴G_{11/2} level, then decays non-radiatively to ²H_{9/2} level and transits to the ground state resulting in ~407 nm violet emission. In addition, Er³⁺ ions at ⁴I_{11/2} level or ⁴F_{7/2} level mutually transfer energy during these transition processes.

Magnetic properties

The $\text{NaYF}_4: \text{Yb}^{3+}/\text{Er}^{3+}$ microcrystals with heavy doping have specific magnetic properties. The magnetization of $\text{NaYF}_4: x\% \text{Yb}^{3+}/2\% \text{Er}^{3+}$ ($x = 18, 38, 78$) microcrystals was recorded using a Lakeshore 7307. It is observed in Fig. 9a that the magnetization of $\text{NaYF}_4: \text{Yb}^{3+}/\text{Er}^{3+}$ microcrystals significantly increases with the increase of Yb^{3+} ions concentration. In general, the ferromagnetism is observed by the hysteresis loop of the magnetization in many published literatures in recent years [23, 24]. Therefore, in order to observe the ferromagnetism, the local amplification of magnetization for the sample Yb^{3+} doping is illustrated in Fig. 9b on the applied magnetic field from -2.5 kOe to 2.5 kOe. However, there is no clear hysteresis loop of the magnetization in Fig. 9b. In other words, the ferromagnetic properties of these microcrystals are not obvious. The magnetic properties of these microcrystals are mainly paramagnetic.

In fact, the up-conversion luminescence efficiency and paramagnetism are competitive in $\text{NaYF}_4: \text{Yb}^{3+}/\text{Er}^{3+}$ microcrystals. The increase of Yb^{3+} ion will lead to the increase of the magnetization of $\text{NaYF}_4: \text{Yb}^{3+}/\text{Er}^{3+}$ microcrystals, but simultaneously leads to the decrease of their luminescent intensity. Therefore, the key is to select the optimal concentration of Yb^{3+} ion for obtaining the expected up-conversion luminescence and paramagnetic property.

CONCLUSION

A series of NaYF_4 microcrystals doped with $\text{Yb}^{3+}/\text{Er}^{3+}$ have been successfully synthesized through a facile hydrothermal method. The XRD and SEM analyses reveal that these optical-magnetic bifunctional microcrystals have relatively uniform size belonging to hexagonal phase at Yb^{3+} ion light doping. On the other hand, the size of the NaYF_4 microcrystals are reduced, with the shape of hexagonal mixed with many cubic-phase microplates at Yb^{3+} ion heavy doping. Under the excitation of 980 nm infrared light, $\text{NaYF}_4: x\% \text{Yb}^{3+}/2\% \text{Er}^{3+}$ ($x = 18, 38, 78$) can emit ~ 657 nm red light from $\text{Er}^{3+} {}^4F_9/2 \rightarrow {}^4I_{15/2}$, ~ 540 nm green light from $\text{Er}^{3+} {}^4F_9/2 \rightarrow {}^4S_{3/2} \rightarrow {}^4I_{15/2}$ and ~ 407 nm violet light from $\text{Er}^{3+} {}^4F_9/2 \rightarrow {}^4I_{15/2}$. In addition, the emission intensities of the three kinds of light are affected by the excitation power and vary with the concentration of Yb^{3+} ion doping. Furthermore, the red emission is more

affected by the Yb^{3+} doping concentration. The ratio of red emission to green emission increases significantly by introducing Yb^{3+} ion heavy doping. The measured results of magnetization reveal that the paramagnetism of the NaYF_4 microcrystals significantly increases with the increase of Yb^{3+} ions concentration. Therefore, up-conversion luminescence and magnetic property in NaYF_4 can be tuned simultaneously by introducing Yb^{3+} ion heavy doping.

Acknowledgements: This work is supported by the National Natural Science Foundation of China (Grant No. 61875054, 61675067, and 61674056).

REFERENCES

- Zhang YH, Zhang LX, Deng RR, Tian J, Zong Y, Jin DY, Liu XG (2014) Multicolor barcoding in a single up-conversion crystal. *J Am Chem Soc* **136**, 4893–4896.
- Gao DL, Zhang XY, Zheng HR, Gao W, He EJ (2013) $\text{Yb}^{3+}/\text{Er}^{3+}$ codoped $\beta\text{-NaYF}_4$ microrods: synthesis and tuning of multicolor up-conversion. *J Alloy Compd* **554**, 395–399.
- Wang J, Deng R, MacDonald MA, Chen BL, Yuan JK, Wang F, Chi DZ, Hor TSA, et al. (2014) Enhancing multiphoton up-conversion through energy clustering at sublattice level. *Nat Mater* **13**, 157–162.
- Liu Y, Yang Q, Ren G, Xu C, Zhang Y (2009) Relationship between microstructure and the achieving of the single-band red up-conversion fluorescence of $\text{Er}^{3+}/\text{Yb}^{3+}$ codoped crystallites. *J Alloy Compd* **467**, 351–356.
- Li W, Tan C, Zhang Y (2013) Simultaneous phase and shape control of monodisperse $\text{NaLuF}_4: \text{Yb}$, Er microcrystals and greatly enhanced up-conversion luminescence from their super-structures. *Opt Commun* **295**, 140–144.
- Huang P, Zheng W, Zhou SY, Tu DT, Chen Z, Zhu HM, Li RF, Ma E, et al. (2014) Lanthanide-doped LiLuF_4 up-conversion nanoprobe for the detection of disease bio-markers. *Angew Chem Int Edit* **53**, 1252–1257.
- Zhou J, Liu Z, Li FY (2012) Up-conversion nanophosphors for small-animal imaging. *Chem Soc Rev* **41**, 1323–1349.
- Cui Y, Zhao S, Liang Z, Han M, Xu Z (2014) Optimized up-conversion emission of $\text{NaLuF}_4: \text{Er}$, Yb nanocrystals codoped with Gd^{3+} ions and its mechanism. *J Alloy Compd* **59**, 330–333.
- Gu ZJ, Yan L, Tian G, Li SJ, Chai ZF, Zhao Y L (2013) Recent advances in design and fabrication of up-conversion nanoparticles and their safe theranostic applications. *Adv Mater* **25**, 3758–3779.
- Zhu HY, Lin M, Jin GR, Lu TJ, Xu F (2017) A modified energy transfer model for determination of

- up-conversion emission of β -NaYF₄:Yb,Er: role of self-quenching effect. *J Lumin* **185**, 29–297.
11. Ding MY, Zhang HL, Chen DQ, Hu QW, Xi J H, Ji ZG (2016) Color-tunable luminescence, energy transfer and temperature sensing behavior of hexagonal NaYF₄:Ce³⁺/b³⁺Tb³⁺/Eu³⁺ microcrystals. *J Alloy Compd* **672**, 117–124.
 12. Wang CY, Cheng XH (2014) Controlled hydrothermal growth and tunable luminescence properties of β -NaYF₄:Yb³⁺/Er³⁺ microcrystals. *J Alloy Compd* **617**, 807–815.
 13. Darani M., Bastani S, Ghahari M, Kardar P (2015) An experimental design approach for hydrothermal synthesis of NaYF₄: Yb³⁺, Tm³⁺ up-conversion microcrystal: UV emission optimization. *Opt Mater* **49**, 255–265.
 14. Liu YX, Zhan S P, Yang QB, Yan ML (2012) Synthesis of biocompatible uniform NaYF₄:Yb³⁺/Er³⁺ nanocrystals and their characteristic photoluminescence. *J Lumin* **132**, 3042–3047.
 15. Liang LL, Liu YM, Zhao XZ (2013) Double-shell β -NaYF₄: Yb³⁺/Er³⁺/SiO₂/TiO₂ submicroplates as a scattering and upconverting layer for efficient dye-sensitized solar cells. *Chem Commun* **49**, 3958–3960.
 16. Yin Z, Zhu YS, Xu W, Wang J, Xu S, Dong B, Xu L, Zhang S, et al(2013) Remarkable enhancement of up-conversion fluorescence and confocal imaging of PMMA Opal/NaYF₄:Yb³⁺, Tm³⁺/Er³⁺ nanocrystals. *Chem Commun* **49**, 3781–3783.
 17. Zhuang JL, Yang XF, Wang J, Lei BF, Liu YL, Wu MM (2016) Additives and solvents-induced phase and morphology modification of NaYF₄ for improving up-conversion emission. *J Solid State Chem* **233**, 178–185.
 18. Tu LP, Liu XM, Wu F, Zhang H (2015) Excitation energy migration dynamics in up-conversion nanomaterials. *Chem Soc Rev* **44**, 1331–1345.
 19. Xia A, Gao Y, Zhou J, Li C, Yang T, Wu D, Wu L, Li F (2011) Core-shell NaYF₄:Yb³⁺,Tm³⁺@FexOy nanocrystals for dual-modality T₂-enhanced magnetic resonance and NIR-to-NIR up-conversion luminescent imaging of small-animal lymphatic node. *Biomaterials* **32**, 7200–7208.
 20. Shen J, Sun L, Zhang YW, Yan CH (2010) Superparamagnetic and up-conversion emitting Fe₃O₄/NaYF₄: Yb,Er hetero-nanoparticles via a crosslinker anchoring strategy. *Chem Commun* **46**, 5731–5733.
 21. Zhu X, Zhou J, Chen M, Shi M, Feng W, Li F (2012) Core-shell Fe₃O₄@NaLuF₄: Yb, Er/Tm nanostructure for MRI, CT and up-conversion luminescence trimodality imaging. *Biomaterials* **33**, 4618–4627.
 22. Wang D, Liu G, Dong X, Wang J (2016) Magnetic-optical-thermal properties assembled into MWCNTs/NaGdF₄:Yb³⁺, Er³⁺ multi-functional nanocomposites. *Colloid Surface A* **490**, 283–290.
 23. Wu XF, Hu SG, Tan CB, Liu YX (2015) Simultaneously optimizing fluorescent and paramagnetic properties of bifunctional NaGdF₄: Yb³⁺/Er³⁺ nanocrystals by crystal field tuning. *Mater Res Bull* **64**, 22–26.
 24. Wu XF, Tang ZJ, Hu SG, Yan HY, Xi ZF, Liu YX (2016) NaLuF₄:Yb³⁺,Er³⁺ bifunctional microcrystals codoped with Gd³⁺ or Dy³⁺ ions: enhanced up-conversion luminescence and ferromagnetic paramagnetic transition. *J Alloy Compd* **684**, 105–111.
 25. Liu Y, Yang Q, Xu C (2009) White up-conversion of rare-earth doped ZnO nanocrystals and its dependence on size of crystal particles and content of Yb³⁺ and Tm³⁺. *J Appl Phys* **105**, 84701–84706.
 26. Tang ZJ, Liu Q, Li J, Wu XF, Zhan SP, Nie GZ, Hu JS, Xi ZF, et al. (2019) Tuning the photothermal effect of NaYF₄:Yb³⁺,Er³⁺ upconversion luminescent crystals through La³⁺ ion doping. *J. Lumin.* **206**, 21–26.
 27. Li K, Liu J, Dimitrije M, Rik VD (2018) Synthesis and up-conversion luminescence properties of a novel Yb³⁺,Er³⁺ co-doped Ca₅Mg₄(VO₄)₆ phosphor. *J Alloy Compd* **737**, 767–773.
 28. Li K, Rik VD (2019) Low-temperature solid-state synthesis and up-conversion luminescence properties in (Na/Li)Bi(MoO₄)₂: Yb³⁺,Er³⁺ and Color Tuning in (Na/Li)Bi(MoO₄)₂: Yb³⁺, Ho³⁺, Ce³⁺ Phosphors. *Inorg Chem* **58**, 6821–6831.